
Deconvolutional Networks on Graph Data

Jia Li¹, Jiajin Li², Yang Liu¹, Jianwei Yu², Yueting Li², Hong Cheng²

¹ Hong Kong University of Science and Technology

² The Chinese University of Hong Kong

jialiee@ust.hk

Abstract

In this paper, we consider an inverse problem in graph learning domain – “given the graph representations smoothed by Graph Convolutional Network (GCN), how can we reconstruct the input graph signal?” We propose Graph Deconvolutional Network (GDN) and motivate the design of GDN via a combination of inverse filters in spectral domain and de-noising layers in wavelet domain, as the inverse operation results in a *high frequency amplifier* and may amplify the noise. We demonstrate the effectiveness of the proposed method on several tasks including graph feature imputation and graph structure generation.

1 Introduction

Graph Convolutional Networks (GCNs) [6, 20] have been widely used to transform an input graph structure A and feature matrix X into graph representations H , which can be taken as a mapping function $f : (A, X) \rightarrow H$. In this paper, we consider its inverse problem $g : (A, H) \rightarrow X$, i.e., *given the graph representations smoothed by GCNs, how can we reconstruct the input graph signal?* More specifically, we initiate a systematic study of Graph Deconvolutional Networks (GDNs), to reconstruct the signals smoothed by GCNs. A good GDN component could benefit many applications such as reconstruction [44] and generation [19]. For examples in computer vision, several studies [45, 29] have demonstrated that the performance of autoencoders on reconstruction and generation can be further improved by encoding with Convolutional Networks and decoding with Deconvolutional Networks [46]. However, extending this symmetric autoencoder framework to graph-structured data requires graph deconvolutional operations, which remains open-ended and hasn’t been well studied as opposed to the large body of solutions that have already been proposed for GCNs.

Most GCNs proposed by prior works, e.g., Cheby-GCN [6] and GCN [20], exploit spectral graph convolutions [33] and Chebyshev polynomials [15] to retain coarse-grained information and avoid explicit eigen-decomposition of the graph Laplacian. Until recently, [39] and [8] have noticed that GCN [20] acts as a *low pass* filter in spectral domain and retains smoothed representations. Inspired by prior works in the domain of signal deconvolution [22, 9, 13], we are motivated to design a GDN by an inverse operation of the *low pass* filters embodied in GCNs. Furthermore, we observe directly reversing a *low pass* filter results in a *high frequency amplifier* in spectral domain and may amplify the noise. In this regard, we introduce a spectral-wavelet GDN to decode the smoothed representations into the input graph signals. The proposed spectral-wavelet GDN employs spectral graph convolutions with an inverse filter to obtain inversed signals and then de-noises the inversed signals in wavelet domain. In addition, we apply Maclaurin series as a fast approximation technique to compute both inverse filters and wavelet kernels [8].

We evaluate the effectiveness of the proposed GDN with two tasks: graph feature imputation [35, 44] and graph structure generation [19, 14]. For the former task, we further propose a graph autoencoder (GAE) framework that resembles the symmetric fashion of architectures [29]. The proposed GAE outperforms the state-of-the-arts on six benchmarks. For the latter task, our proposed GDN can

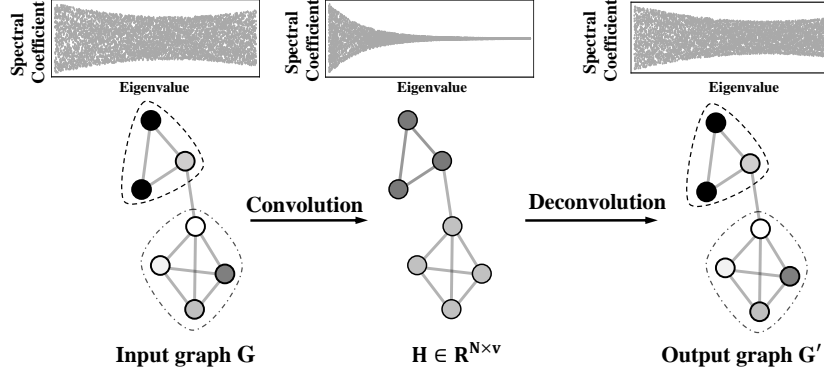


Figure 1: Schematic diagram of the graph autoencoder perspective. We plot graphs in spatial domain together with their signal coefficients in spectral domain. In the encoding stage, we run a GCN model to derive smoothed node representations. In the decoding stage, we reconstruct the graph signal via a GDN model.

enhance the generation performance of popular variational autoencoder frameworks including VGAE [19] and Graphite [14].

The contributions of this work are summarized as follows:

- We propose Graph Deconvolutional Network (GDN), the opposite operation of Graph Convolutional Network (GCN) that reconstructs graph signals from smoothed node representations.
- We study GDN from the perspective of inverse operations in spectral domain and identify the inverse operation results in a *high frequency amplifier* and may amplify the noise. To solve the noise issue, a de-noising process based on graph wavelet is further proposed.

2 Preliminaries

In this work, we are given an undirected, unweighted graph $G = (V, A, X)$. V is the node set and $N = |V|$ denotes the number of nodes. The adjacency matrix $A \in \mathbb{R}^{N \times N}$ represents the graph structure. The feature matrix $X \in \mathbb{R}^{N \times d}$ represents the node attributes.

2.1 Convolution on graphs

The convolutional layers are used to derive smoothed node representations, such that nodes that are similar in topological space should be close enough in Euclidean space. Formally, the spectral graph convolution on a signal $x \in \mathbb{R}^N$ is defined as:

$$h = g_c * x = U \text{diag}(g_c(\lambda_1), \dots, g_c(\lambda_N)) U^\top x, \quad (1)$$

where $\{\lambda_i\}_{i=1}^N$ are the eigenvalues of the normalized Laplacian matrix $L_{sym} = D^{-\frac{1}{2}} L D^{-\frac{1}{2}}$, L and D are the Laplacian and degree matrices of the input graph A respectively, and U is the eigenvector matrix of $L_{sym} = U \Lambda U^\top$. In this work, we focus on GCN [20], one of the popular convolution operations on graphs:

$$H = \text{GCN}(A, X), \quad (2)$$

where $H \in \mathbb{R}^{N \times v}$ denotes smoothed node representations. Specifically, [39] show that GCN is a *low pass* filter in spectral domain with $g_c(\lambda_i) = 1 - \lambda_i$, i.e.,

$$h_c = \sigma(U \text{diag}(g_c(\lambda)) U^\top x), \quad (3)$$

where $\sigma(\cdot)$ is the activation function.

2.2 Deconvolution on graphs

The deconvolutional layers are used to recover the original graph features given smoothed node representations. Formally, the spectral graph deconvolution on the smoothed representation $h \in \mathbb{R}^N$ is defined as:

$$x' = g_d * h = U \text{diag}(g_d(\lambda_1), \dots, g_d(\lambda_N)) U^\top h, \quad (4)$$

With this deconvolution operation, we can use GDNs to produce fine-grained graph signals from the encoded H .

$$X' = \text{GDN}(A, H), \quad (5)$$

where $X' \in \mathbb{R}^{N \times d}$ denotes the recovered graph features. We shall further discuss our design of GDN in Section 3.

From the perspective of encoder-decoder, the convolution operation could be used as an encoder and the deconvolution operation as a decoder. We show a schematic diagram of this encoder-decoder perspective in Figure 1.

3 Graph Deconvolutional Network

In this section, we present our design of GDN. Motivated by prior works in signal deconvolution [16], a naive deconvolutional net can be obtained using the inverse filter $g_c^{-1}(\lambda_i) = \frac{1}{1-\lambda_i}$ in spectral domain. Unfortunately, the naive deconvolutional net results in a *high frequency amplifier* and may amplify the noise [9, 13]. This point is obvious for $g_c^{-1}(\lambda_i)$ as the signal fluctuates near $\lambda_i = 1$ if noise exists.

3.1 Noise analysis

Our target is to recover the original graph features given smoothed node representations h_c encoded by GCN [20]. Without the noise, it is naive to obtain the closed-form recovery relationship by the inverse operation $g_c^{-1}(\lambda) = \frac{1}{1-\lambda}$ directly, i.e.,

$$x = U \text{diag}(g_c^{-1}(\lambda)) U^\top \sigma^{-1}(h_c), \quad (6)$$

Here, we assume the activation function $\sigma(\cdot)$ is an inverse operator, e.g., Leaky ReLU, sigmoid, tanh. Actually, it is quite reasonable to consider such a prototypical model of invertible networks in the theoretical analysis. Otherwise, we need to address an ill-posed inverse problem instead as we automatically lose some information (e.g., null space). Hence, it is impossible to recover the ground-truth even under the noiseless model, see [1] for details.

Graph noise is ubiquitous in real-world applications. Following the convention in signal deconvolution [9] and image restoration [13], let's consider the white noise model, i.e., \hat{h} is the smoothed node representations mixed with graph convolution and white noise,

$$\hat{h} = \sigma(U \text{diag}(g_c(\lambda)) U^\top x) + \epsilon, \quad (7)$$

where ϵ is the white Gaussian noise (i.e., $\epsilon \sim \mathcal{N}(0, \sigma^2 \mathbb{I}_N)$).

Next, we show that it will amplify the noise if we apply the inverse operation to the white noise model directly. That is,

$$x' = U \text{diag}(g_c^{-1}(\lambda)) U^\top \sigma^{-1}(\hat{h}), \quad (8)$$

Proposition 1. *Considering the independent white noise model (7) and (8), if the inversed activation function is deferentiable which satisfies $\partial \sigma^{-1}(0) \geq 1$, the variance of x' is larger than the white noised ϵ added on the generative model.*

It was worthwhile mentioning that the condition regarding the inverse operator $\partial \sigma^{-1}(0) \geq 1$ is quite reasonable. Actually, it holds for many representative activation functions, including sigmoid, tanh and Leaky ReLU. Please refer to Appendix A for details. Proposition 1 shows the proposed inverse operation may introduce undesirable noise into the output graph. Thus, a de-noising process is necessary thereafter.

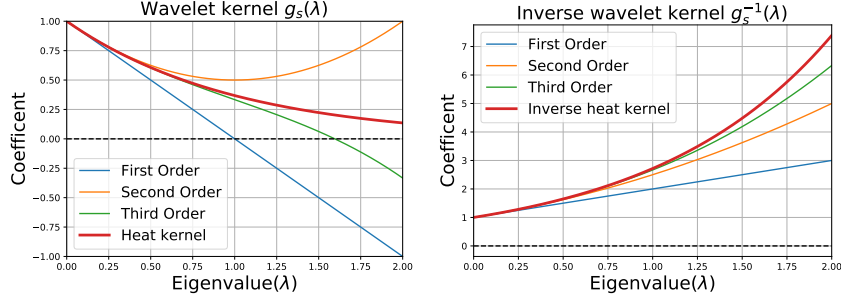


Figure 2: Low-order Maclaurin Series well approximate wavelet kernel and inverse wavelet kernel with $s = 1$.

3.2 The proposed GDN

To ameliorate the noise issue, we propose an efficient, hybrid spectral-wavelet deconvolutional network that performs inverse signal recovery in spectral domain first, and then conducts a de-noising step in wavelet domain to remove the amplified noise [28].

3.2.1 Inverse operator

Regarding the inverse operation in (6), the core is to explicitly compute eigen-decomposition. We propose to apply Maclaurin series approximation on $g_c^{-1}(\Lambda) = \sum_{n=0}^{\infty} \Lambda^n$ and get a fast algorithm as below:

$$U \text{diag}(g_c^{-1}(\lambda))U = \sum_{n=0}^{\infty} L_{sym}^n. \quad (9)$$

A detailed derivative of (9) can be found in Appendix E. When truncated low order approximation is used in practice with $n \leq 3$ [6], we derive a spectral filter with $g_c^{-1}(\lambda_i) = 1 + \lambda_i + \lambda_i^2 + \lambda_i^3$.

Following [29], we can use another activation function and trainable parameter matrix to estimate σ^{-1} , to avoid the potential non-invertible problem. Thus, the inverse operator becomes:

$$M = \sigma((I_N + \sum_{n=1}^3 L_{sym}^n)HW_3), \quad (10)$$

where W_3 is the parameter set to be learned.

We contrast the difference between inverse operator in this work and other reconstruction methods including [47] and GALA [30].

Inverse operator vs. GCN decoder [47] Compared with GCN decoder [47] which directly uses GCN for signal reconstruction, the proposed inverse operator demonstrates its efficacy in recovering the high frequency signals of the graph, as shown in Figure 3 (b). We shall further discuss this point in Section 3.3.

Inverse operator vs. GALA GALA [30] can be viewed as the first-order approximation towards inverse operator in this work, with a spectral kernel of $1 + \lambda_i$. The difference is that our inverse operator can well approximate the inverse filter $g_c^{-1}(\lambda_i) = \frac{1}{1-\lambda_i}$ with third-order polynomials.

3.2.2 Wavelet de-noising

Wavelet-based methods have a strong impact on the field of de-noising, especially in image restoration when noise is amplified by inverse filters [28]. In the literature, many wavelet de-noising methods have been proposed, e.g., SureShrink [9], BayesShrink [5], and they differ in how they estimate the separating threshold. Our method generalizes these threshold ideas and automatically separates the noise from the useful information with a learning-based approach. Consider the input signal of wavelet system is mixed with Gaussian noise, the reasons why wavelet denoising works are: (1) a graph wavelet basis holds the majority of signal energy into a small number of large coefficients,

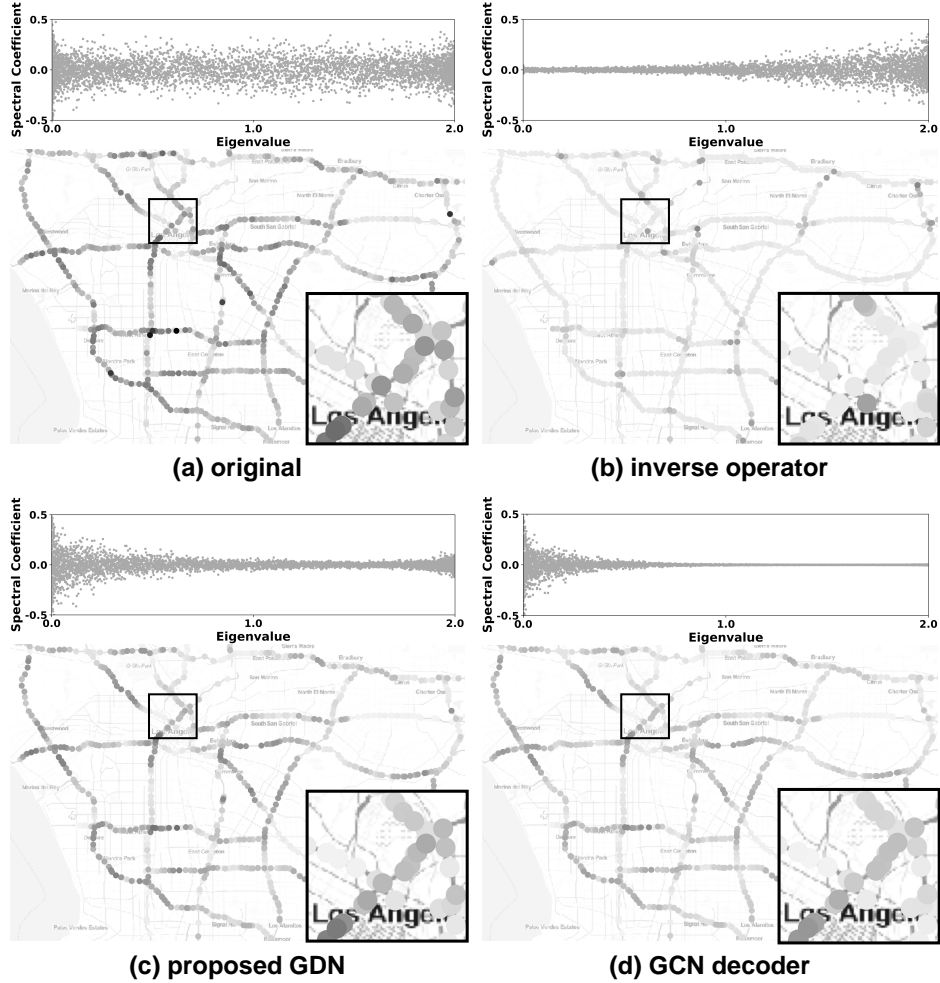


Figure 3: Illustration of road occupancy rates decoded by different approaches (zoom in to see details). A darker color implies a higher road occupancy rate. In each figure above, we plot the reconstructed signal in spatial domain together with coefficients in spectral domain. (a) the original, (b) inverse operator (RMSE = 0.11), (c) GDN/our model (RMSE = 0.07), (d) GCN decoder [47] (RMSE = 0.09).

and (2) Gaussian noise in the original graph domain is again a Gaussian noise in wavelet domain (with the same amplitude), see [16] for details. The core thus becomes how we can separate a small number of large coefficients and the noise in wavelet domain. Given the latter is unknown, we adopt a trainable parameter matrix to linearly transform the noise under zero and useful coefficients bigger than zero, where ReLU is used to eliminate the noise.

Consider a set of wavelet bases $\Psi_s = (\Psi_{s1}, \dots, \Psi_{sN})$, where each one Ψ_{si} denotes a signal on graph diffused away from node i and s is a scaling parameter [40], the wavelet bases can be written as $\Psi_s = U g_s(\Lambda) U^\top$ and $g_s(\cdot)$ is a filter kernel. Following previous works GWNN [40] and GRAPHWAVE [8], we use the heat kernel $g_s(\lambda_i) = e^{-s\lambda_i}$, as heat kernel admits easy calculation of inverse wavelet transform with $g_s^{-1}(\lambda_i) = e^{s\lambda_i}$. In addition, we can apply Maclaurin series approximation on heat kernel and neglect explicit eigen-decomposition by:

$$\Psi_s = \sum_{n=0}^{\infty} \frac{(-1)^n}{n!} s^n L_{sym}^n, \quad (11)$$

$$\Psi_s^{-1} = \sum_{n=0}^{\infty} \frac{s^n}{n!} L_{sym}^n, \quad (12)$$

To cope with the noise threshold estimation problem, we introduce a parameterized matrix in wavelet domain and eliminate these noise coefficients via a ReLU function, in the hope of learning a separating threshold from the data itself. Together with the representation M raised in Section 3.2.1, we derive the reconstructed signal as:

$$X' = \Psi_s \text{ReLU}(\Psi_s^{-1} M W_4) W_5, \quad (13)$$

where W_4 and W_5 are trainable parameters.

We then contrast the difference between Wavelet Neural Network (WNN) in this work and other related WNNs including GWNN [40] and GRAPHWAVE [8].

Scalability An important issue in WNN is that one needs to avoid explicit eigen-decomposition to compute wavelet bases for large graphs. Both GRAPHWAVE and GWNN, though trying to avoid eigen-decomposition by exploiting Chebyshev polynomials, still rely integral operations (see Appendix D in [40]) and there is no clear way to scale up. Differently, we use Maclaurin series to approximate wavelet bases, which has explicit polynomial coefficients and can resemble the heat kernel well when $n = 3$. Please refer to Figure 2 for more details.

De-noising The purpose of both GWNN and GRAPHWAVE is to derive node presentations with localized graph convolution and flexible neighborhood, such that downstream tasks like classification can be simplified. On the contrary, our work implements wavelet neural network in the purpose of detaching the useful information and the noise amplified by inverse operator. Due to the different purpose, our work applies the activation function in wavelet domain while GWNN in the original vertex domain.

3.3 Visualization

In Figure 3, we illustrate the difference between GDN and each component inside by visualizing the reconstructed road occupancy rates in a traffic network. The traffic network targets District 7 of California collected from Caltrans Performance Measurement System (PeMS)¹. We select 4438 sensor stations as the node set V and collect their road average occupancy rates at 5pm on June 24, 2020. Following [23], we construct an adjacency matrix A by denoting $A_{ij} = 1$ if sensor station v_j and v_i are adjacent on a freeway along the same direction. We reconstruct road occupancy rate of each sensor station with three decoder variants: (b) inverse operator, (c) our proposed GDN, (d) GCN decoder [47]. Here the three variants share the same encoders.

As can be seen, while both GDN and GCN decoders can resemble the input signal in low frequency, GDN decoder retains more high frequency information. For inverse operator decoder, although keeping much high frequency information (mixed with noise), it drops lots of low frequencies, making the decoded signals less similar to the input in Euclidean space.

4 Experiments

We validate the proposed GDN on graph feature imputation [35, 44] and graph generation [19, 14]. The former task reconstructs graph features and the latter generates graph structures.

4.1 Graph feature imputation

In our model, we consider feature imputation as feature recovery on graphs. The model is trained on an incomplete version of feature matrix (training data) and further used to infer the potential missing features (test data).

Datasets We use six benchmark datasets including several domains: citation networks (Cora, Citeseer) [32], product co-purchase networks (Amaphoto, Amacomp) [26], social rating networks (Douban, Ciao²). For citation networks and product co-purchase networks, we use the preprocessed versions provided by [35] with uniform randomly missing rate of 10%. For Douban, we use the preprocessed dataset provided by [27]. For Ciao, we use a sub-matrix of 7,317 users and 1,000 items. Dataset statistics are summarized in Table 3 in the Appendix.

¹<http://pems.dot.ca.gov/>

²<https://www.ciao.co.uk/>

Table 1: RMSE test comparison of different methods on graph feature imputation

Datasets	Ciao	Douban	Cora	Citeseer	Amaphoto	Amacomp
MEAN	1.385	0.850	0.503	0.503	0.414	0.417
KNN	1.461	0.817	0.459	0.443	0.421	0.422
SVD [37]	1.380	0.833	0.493	0.490	0.413	0.417
MICE [4]	1.600	-	0.480	-	0.481	0.487
GAIN [43]	1.099	0.809	0.433	0.421	0.420	0.416
GRAPE [44]	1.042	0.742	0.430	0.419	0.399	0.402
Inverse decoder	1.115	0.812	0.447	0.431	0.409	0.407
GCN decoder[47]	1.132	0.826	0.439	0.434	0.410	0.409
GALA [30]	1.147	0.833	0.457	0.435	0.415	0.411
OURS	1.011	0.734	0.415	0.399	0.391	0.393

Setup Our graph autoencoder framework consists of an encoder and a decoder. Our encoder consists of two layers of Graph Convolutional Networks (GCN) [20]. Our decoder consists of one layer of proposed GDN, to produce fine-grained graphs. We use the Mean Squared Error (MSE) loss to reconstruct the features. We run 5 trials with different seeds and report the mean of the results. For detailed architecture, please refer to Appendix C. For detailed hyper-parameter settings, please refer to Appendix D. We report Root Mean Squared Error (RMSE).

Baselines We compare with three commonly used imputation methods and three deep learning based imputation models:

- **MEAN**, which replaces the missing feature entries with the mean values of all observed feature entries.
- **KNN**, which first identifies the k-nearest neighbor samples and imputes the missing feature entries with the mean entries of these k samples. We set $k = 5$ in this work.
- **SVD** [37], which replaces the missing feature entries based on matrix completion with iterative low-rank SVD decomposition.
- **MICE** [4], which is a multiple regression method that infers missing entries by Markov chain Monte Carlo (MCMC) techniques.
- **GAIN** [43], which is a deep learning imputation model with generative adversarial training.
- **GRAPE** [44], which is the state-of-the-art deep learning imputation model based on deep graph representations.

For ablation studies of the graph autoencoder framework specified in Appendix C, we also include the results of decoders using GCN decoder [47], GALA [30], and inverse decoder in Section 3.2.1, to be compared with our proposed GDN. Besides, we compare with popular matrix completion methods in Appendix B for discrete feature recovery.

Results The test RMSE on the six benchmarks are shown in Table 1. Our method performs the best on all datasets, e.g., it beats the second best model GRAPE by 0.02 on Citeseer and 0.031 on Ciao, which shows the superiority of our methods on feature imputation. The feature imputation RMSE with respect to different missing rate is shown in Figure 4. As can be seen, our method performs the best with respect to different missing rate, e.g., it achieves 0.016 improvement over the second best model GRAPE on Citeseer when the missing rate is 70%, and 0.007 improvement over the second best model GRAPE on Amacomp when the missing rate is 30%.

Ablation study We investigate the role of wavelet de-noising in our GDN. We let the four decoder variants share the same depth of layers and parameter size. As observed in Table 1, when decoding by inverse operator, the performance is on a par with that of GCN decoders [47] and outperformed by our GDN decoders on all six datasets, indicating the effectiveness of this hybrid design. The performance of inverse decoder specified in Section 3.2.1 is always better than that of GALA [30], which shows the superiority of our third-order approximation.

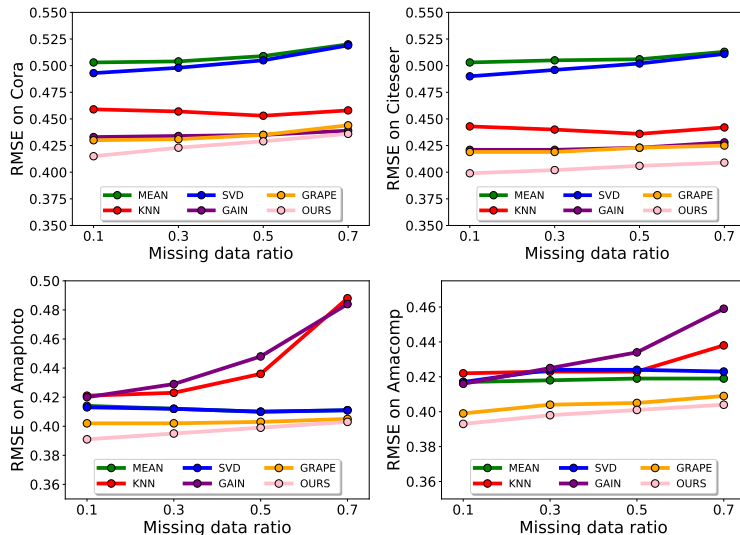


Figure 4: Comparison of different methods on graph feature imputation tasks. The x-axis denotes the missing ratio while the y-axis denotes RMSE on test set.

Table 2: The effect of GDN with various graph generation methods

Datasets	MUTAG			PTC-MR			ZINC		
	$\log p(A Z)$	AUC	AP	$\log p(A Z)$	AUC	AP	$\log p(A Z)$	AUC	AP
VGAE [19]	-1.101	0.716	0.427	-1.366	0.566	0.433	-1.035	0.556	0.288
VGAE + GDN	-1.026	0.823	0.611	-1.351	0.760	0.602	-1.006	0.858	0.611
Graphite [14]	-1.100	0.732	0.447	-1.362	0.564	0.437	-1.039	0.553	0.288
Graphite + GDN	-1.024	0.818	0.608	-1.347	0.773	0.613	-0.998	0.838	0.567

4.2 Graph structure generation

Data and baselines We use three molecular graphs: MUTAG [21] containing mutagenic compounds, PTC-MR [21] containing compounds tested for carcinogenicity and ZINC [17] containing druglike organic molecules, to evaluate the performance of GDN on graph generation. Dataset statistics are summarized in Table 4 in the Appendix. We test GDN on two popular variational autoencoder framework including VGAE [19] and Graphite [14]. Our purpose is to validate if GDN helps with the generation performance.

Setup For VGAE and Graphite, we reconstruct the graph structures using their default methods and the features using GDN. The two reconstructions share the same encoders and sample from the same latent distributions. For detailed architecture, please refer to Appendix D. We train for 200 iterations with a learning rate of 0.01. For MUTAG and PTC-MR, we use 50% samples as train set and the remaining 50% as test set. For ZINC, we use the default train-test split.

Results Evaluating the sample quality of generative models is challenging [36]. In this work, we validate the generative performance with the log-likelihood ($\log p(A|Z)$), area under the receiver operating characteristics curve (AUC) and average precision (AP). As shown in Table 2, GDN can improve the generative performance of both VGAE and Graphite in general, e.g., it improve the AP score of Graphite by 16.1% on MUTAG, the AUC score of Graphite by 20.9% on PTC-MR and $\log p(A|Z)$ of VGAE by 0.029 on ZINC, which shows the superiority of GDN.

5 Related work

Deconvolutional networks The area of signal deconvolution [22] has a long history in the signal processing community and is about the process of estimating the true signals given the degraded or smoothed signal characteristics [2]. Later deep learning studies [46, 29] consider deconvolutional

networks as the opposite operation for Convolutional Neural Networks (CNNs) and have mainly focused on Euclidean structures, e.g., image. For deconvolutional networks on non-Euclidean structures like graphs, the study is still sparse. [12] proposes the network deconvolution as inferring the true network given partially observed structure. [42] formulates the deconvolution as a pre-processing step on the observed signals, in order to improve classification accuracy. [47] considers recovering graph signals from the latent representation. However, it just adopts the filter design used in GCN and sheds little insight into the internal operation of GDN.

Graph autoencoders Since the introduction of Graph Neural Networks (GNNs) [20, 6] and autoencoders (AEs), many studies [19, 14] have used GNNs and AEs to encode to and decode from latent representations. Although some encouraging progress has been achieved, there is still no work about graph deconvolution that can up-sample latent feature maps to restore their original resolutions. In this regard, current graph autoencoders bypass the difficulty via (1) non-parameterized decoders [19, 7, 24], (2) GCN decoders [14], (3) multi-layer perceptron (MLP) decoders [34], and (4) Laplacian sharpening [30].

Graph feature imputation Feature imputation techniques can be generally classified into two groups: statistical approaches and deep learning models. The former group includes KNN, SVD [37], MICE [4], in which they makes assumptions about the data distribution through a parametric density function. The latter group includes GAIN [43], GRAPE [44]. Recently GRAPE [44] proposes graph feature imputation that assumes a network among items and the network is helpful in boosting the feature imputation performance. A related topic is matrix completion [27, 3, 11] in which it usually makes the assumption of finite and discrete feature values. Differently, both GRAPE and our method can recover both continuous and discrete feature values.

Graph structure generation Graph structure generation techniques can be classified into three groups: one-shot [19, 14, 34], substructure [18] and node-by-node [25]. As this work is more related to the group of one-shot, we refer the readers to [10] for the details of other groups. The group of one-shot generates the entire graph all at once. Representative works include VGAE [19], Graphite [14] and GraphVAE [34]. Both VGAE and Graphite reconstruct graphs based on the similarities of graph structures. Differently, GraphVAE considers both the similarities of structures and node features and reconstructs node features using MLP. In this work, we show that the performance of one-shot graph generators can be improved by reconstructing node features using GDN.

6 Conclusion

In this paper, we present Graph Deconvolutional Network (GDN), the opposite of GCN that recovers graph signals from smoothed representations. The introduced GDN uses spectral graph convolutions with an *inverse* filter to obtain inversed signals and then de-noises the inversed signals in wavelet domain. The effectiveness of the proposed method is validated on graph feature imputation and graph structure generation tasks.

7 Limitation

Broadly speaking, graph signal restoration is an ill-posed problem. In this regard, the prior knowledge is important for high-quality recovery. This paper only pays attention to vanilla GCN [20] (Kipf & Welling, 2017) and it is not clear whether the spectral-wavelet GDN ideas can be applied to other GNNs, e.g., GAT [38], GIN [41]. Another limitation of this work is that the heat kernel in wavelet parts is not a band-pass filter, as it should be.

8 Broader Impact

This work initiates the restoration of graph signals smoothed by vanilla GCN [20] (Kipf & Welling, 2017). As a sequence, researchers in drug design or molecule generation may benefit from this research, since the visualization and understanding of GCN based representations is worthwhile to be further explored.

Acknowledgments and Disclosure of Funding

The work was supported by NSFC Grant No. U1936205 and General Research Fund from the Research Grant Council of the Hong Kong Special Administrative Region, China [Project No.: CUHK 14205618].

References

- [1] Lynton Ardizzone, Jakob Kruse, Sebastian Wirkert, Daniel Rahner, Eric W Pellegrini, Ralf S Klessen, Lena Maier-Hein, Carsten Rother, and Ullrich Köthe. “Analyzing inverse problems with invertible neural networks”. In: *ICLR* (2019).
- [2] Mark R Banham and Aggelos K Katsaggelos. “Digital image restoration”. In: *IEEE signal processing magazine* 14.2 (1997), pp. 24–41.
- [3] Rianne van den Berg, Thomas N Kipf, and Max Welling. “Graph convolutional matrix completion”. In: *SIGKDD* (2018).
- [4] Stef Buuren and Catharina Groothuis-Oudshoorn. “MICE: Multivariate Imputation by Chained Equations in R”. In: *Journal of Statistical Software* 45 (Dec. 2011).
- [5] S Grace Chang, Bin Yu, and Martin Vetterli. “Adaptive wavelet thresholding for image denoising and compression”. In: *IEEE transactions on image processing* 9.9 (2000), pp. 1532–1546.
- [6] Michaël Defferrard, Xavier Bresson, and Pierre Vandergheynst. “Convolutional neural networks on graphs with fast localized spectral filtering”. In: *Advances in neural information processing systems*. 2016, pp. 3844–3852.
- [7] Chenhui Deng, Zhiqiang Zhao, Yongyu Wang, Zhiru Zhang, and Zhuo Feng. “Graphzoom: A multi-level spectral approach for accurate and scalable graph embedding”. In: *ICLR* (2020).
- [8] Claire Donnat, Marinka Zitnik, David Hallac, and Jure Leskovec. “Learning structural node embeddings via diffusion wavelets”. In: *ACM SIGKDD Conference on Knowledge Discovery and Data Mining (KDD)*. 2018, pp. 1320–1329.
- [9] David L Donoho and Jain M Johnstone. “Ideal spatial adaptation by wavelet shrinkage”. In: *biometrika* 81.3 (1994), pp. 425–455.
- [10] Faezeh Faez, Yassaman Ommi, Mahdiah Soleymani Baghshah, and Hamid R Rabiee. “Deep Graph Generators: A Survey”. In: *arXiv preprint arXiv:2012.15544* (2020).
- [11] Wenqi Fan, Yao Ma, Qing Li, Yuan He, Eric Zhao, Jiliang Tang, and Dawei Yin. “Graph Neural Networks for Social Recommendation”. In: *The World Wide Web Conference*. ACM, 2019, pp. 417–426.
- [12] Soheil Feizi, Daniel Marbach, Muriel Médard, and Manolis Kellis. “Network deconvolution as a general method to distinguish direct dependencies in networks”. In: *Nature biotechnology* 31.8 (2013), pp. 726–733.
- [13] Mário AT Figueiredo and Robert D Nowak. “An EM algorithm for wavelet-based image restoration”. In: *IEEE Transactions on Image Processing* 12.8 (2003), pp. 906–916.
- [14] Aditya Grover, Aaron Zweig, and Stefano Ermon. “Graphite: Iterative generative modeling of graphs”. In: *The International Conference on Machine Learning (ICML)*. 2019, pp. 2434–2444.
- [15] David K Hammond, Pierre Vandergheynst, and Rémi Gribonval. “Wavelets on graphs via spectral graph theory”. In: *Applied and Computational Harmonic Analysis* 30.2 (2011), pp. 129–150.
- [16] Jeff Irion and Naoki Saito. “Efficient approximation and denoising of graph signals using the multiscale basis dictionaries”. In: *IEEE Transactions on Signal and Information Processing over Networks* 3.3 (2016), pp. 607–616.
- [17] John J Irwin, Teague Sterling, Michael M Mysinger, Erin S Bolstad, and Ryan G Coleman. “ZINC: a free tool to discover chemistry for biology”. In: *Journal of chemical information and modeling* 52.7 (2012), pp. 1757–1768.
- [18] Wengong Jin, Regina Barzilay, and Tommi Jaakkola. “Junction tree variational autoencoder for molecular graph generation”. In: *The International Conference on Machine Learning (ICML)* (2018).

- [19] Thomas N Kipf and Max Welling. “Variational Graph Auto-Encoders”. In: *Conference on Neural Information Processing Systems (NeurIPS) Workshop on Bayesian Deep Learning*. 2016.
- [20] Thomas N. Kipf and Max Welling. “Semi-Supervised Classification with Graph Convolutional Networks”. In: *The International Conference on Learning Representations (ICLR)*. 2017.
- [21] Nils Kriege and Petra Mutzel. “Subgraph matching kernels for attributed graphs”. In: *ICML* (2012), pp. 291–298.
- [22] Deepa Kundur and Dimitrios Hatzinakos. “Blind image deconvolution”. In: *IEEE signal processing magazine* 13.3 (1996), pp. 43–64.
- [23] Jia Li, Zhichao Han, Hong Cheng, Jiao Su, Pengyun Wang, Jianfeng Zhang, and Lujia Pan. “Predicting Path Failure In Time-Evolving Graphs”. In: *Proceedings of the 25th ACM SIGKDD International Conference on Knowledge Discovery and Data Mining (KDD)*. 2019.
- [24] Jia Li, Jianwei Yu, Jiajin Li, Honglei Zhang, Kangfei Zhao, Yu Rong, Hong Cheng, and Junzhou Huang. “Dirichlet Graph Variational Autoencoder”. In: *Neurips*. 2020.
- [25] Qi Liu, Miltiadis Allamanis, Marc Brockschmidt, and Alexander L. Gaunt. “Constrained Graph Variational Autoencoders for Molecule Design”. In: *The Thirty-second Conference on Neural Information Processing Systems* (2018).
- [26] Julian McAuley, Christopher Targett, Qinfeng Shi, and Anton Van Den Hengel. “Image-based recommendations on styles and substitutes”. In: *SIGIR*. 2015, pp. 43–52.
- [27] Federico Monti, Michael Bronstein, and Xavier Bresson. “Geometric matrix completion with recurrent multi-graph neural networks”. In: *Neurips*. 2017, pp. 3697–3707.
- [28] Ramesh Neelamani, Hyeokho Choi, and Richard Baraniuk. “ForWaRD: Fourier-wavelet regularized deconvolution for ill-conditioned systems”. In: *IEEE Transactions on signal processing* 52.2 (2004), pp. 418–433.
- [29] Hyeonwoo Noh, Seunghoon Hong, and Bohyung Han. “Learning deconvolution network for semantic segmentation”. In: *Proceedings of the IEEE international conference on computer vision*. 2015, pp. 1520–1528.
- [30] Jiwoong Park, Minsik Lee, Hyung Jin Chang, Kyuewang Lee, and Jin Young Choi. “Symmetric graph convolutional autoencoder for unsupervised graph representation learning”. In: *Proceedings of the IEEE/CVF International Conference on Computer Vision*. 2019, pp. 6519–6528.
- [31] Yu Rong, Wenbing Huang, Tingyang Xu, and Junzhou Huang. “DropEdge: Towards Deep Graph Convolutional Networks on Node Classification”. In: *International Conference on Learning Representations*. 2020. URL: <https://openreview.net/forum?id=Hkx1qkrKPr>.
- [32] P. Sen, G. Namata, M. Bilgic, L. Getoor, B. Galligher, and T. Eliassi-Rad. “Collective classification in network data”. In: *AI magazine* 29.3 (2008), pp. 93–106.
- [33] David I Shuman, Sunil K Narang, Pascal Frossard, Antonio Ortega, and Pierre Vandergheynst. “The emerging field of signal processing on graphs: Extending high-dimensional data analysis to networks and other irregular domains”. In: *IEEE signal processing magazine* 30.3 (2013), pp. 83–98.
- [34] Martin Simonovsky and Nikos Komodakis. “Graphvae: Towards generation of small graphs using variational autoencoders”. In: *International Conference on Artificial Neural Networks*. Springer. 2018, pp. 412–422.
- [35] Hibiki Taguchi, Xin Liu, and Tsuyoshi Murata. “Graph convolutional networks for graphs containing missing features”. In: *Future Generation Computer Systems* 117 (2021), pp. 155–168.
- [36] Lucas Theis, Aäron van den Oord, and Matthias Bethge. “A note on the evaluation of generative models”. In: *ICLR* (2016).
- [37] Olga Troyanskaya, Mike Cantor, Gavin Sherlock, Trevor Hastie, Rob Tibshirani, David Botstein, and Russ Altman. “Missing Value Estimation Methods for DNA Microarrays”. In: *Bioinformatics* 17 (July 2001), pp. 520–525. DOI: 10.1093/bioinformatics/17.6.520.
- [38] Petar Veličković, Guillem Cucurull, Arantxa Casanova, Adriana Romero, Pietro Lio, and Yoshua Bengio. “Graph attention networks”. In: *ICLR* (2018).
- [39] Felix Wu, Amauri Souza, Tianyi Zhang, Christopher Fifty, Tao Yu, and Kilian Weinberger. “Simplifying Graph Convolutional Networks”. In: *Proceedings of the 36th International Conference on Machine Learning (ICML)*. PMLR, 2019, pp. 6861–6871.

- [40] Bingbing Xu, Huawei Shen, Qi Cao, Yunqi Qiu, and Xueqi Cheng. “Graph wavelet neural network”. In: *The International Conference on Learning Representations (ICLR)* (2019).
- [41] Keyulu Xu, Weihua Hu, Jure Leskovec, and Stefanie Jegelka. “How powerful are graph neural networks?” In: *ICLR* (2019).
- [42] Jingkang Yang and Santiago Segarra. “Enhancing geometric deep learning via graph filter deconvolution”. In: *2018 IEEE Global Conference on Signal and Information Processing (GlobalSIP)*. IEEE. 2018, pp. 758–762.
- [43] Jinsung Yoon, James Jordon, and Mihaela van der Schaar. “GAIN: Missing Data Imputation using Generative Adversarial Nets”. In: *Proceedings of the 35th International Conference on Machine Learning, ICML 2018, Stockholmsmässan, Stockholm, Sweden, July 10-15, 2018*. Ed. by Jennifer G. Dy and Andreas Krause. Vol. 80. Proceedings of Machine Learning Research. PMLR, 2018, pp. 5675–5684.
- [44] Jiaxuan You, Xiaobai Ma, Daisy Ding, Mykel Kochenderfer, and Jure Leskovec. “Handling Missing Data with Graph Representation Learning”. In: *NeurIPS* (2020).
- [45] Matthew D Zeiler and Rob Fergus. “Visualizing and understanding convolutional networks”. In: *European conference on computer vision*. Springer. 2014, pp. 818–833.
- [46] Matthew D Zeiler, Dilip Krishnan, Graham W Taylor, and Rob Fergus. “Deconvolutional networks”. In: *2010 IEEE Computer Society Conference on computer vision and pattern recognition*. IEEE. 2010, pp. 2528–2535.
- [47] Chun-Yang Zhang, Junfeng Hu, Lin Yang, CL Philip Chen, and Zhiliang Yao. “Graph deconvolutional networks”. In: *Information Sciences* 518 (2020), pp. 330–340.

Table 3: Statistics of the datasets used in graph feature imputation

Dataset	Nodes	Train/Test Features	Feature Density	Edges	Edge Density
Douban	3,000	123,202/13,689	1.52%	2,690	0.03%
Ciao	7,317	39,279/16,892	0.77%	111,781	0.21%
Cora	2,708	88,590/9,842	2.54%	5,429	0.15%
Citeseer	3,327	189,298/21,032	1.70%	4,732	0.08%
Amaphoto	7,650	35,640/3,958	0.69%	143,663	0.49%
Amacomp	13,752	66,150/7,350	0.69%	287,209	0.30%

Table 4: Statistics of the datasets used in graph structure generation

Datasets	MUTAG	PTC-MR	ZINC
No.Graphs	188	344	250k
Avg.Nodes	17.9	14.3	23.1
Avg.Edges	19.8	14.7	23.9

A Proof of Proposition 1

Proof. Based on the independent white noise model (7) and (8), we have

$$\begin{aligned}
x' &= U \text{diag}(g_c^{-1}(\lambda)) U^\top \sigma^{-1}(\hat{h}) \\
&= U \text{diag}(g_c^{-1}(\lambda)) U^\top \sigma^{-1}(\sigma(U \text{diag}(g_c(\lambda)) U^\top x) + \epsilon) \\
&= x + U \text{diag}(g_c^{-1}(\lambda)) U^\top \sigma^{-1}(\epsilon).
\end{aligned}$$

Hence,

$$(x' - x) = U \text{diag}(g_c^{-1}(\lambda)) U^\top \sigma^{-1}(\epsilon). \quad (14)$$

In general, we cannot find an exact formula for the variance of a nonlinear function. Here, we consider a more relevant case, that is, a random variable ϵ is fairly closed to the mean (i.e., the standard error is sufficiently small), then we can approximate the nonlinear transformation $\sigma^{-1}(\epsilon)$ with a first-order Taylor expansion. Under the condition $\sigma^{-1}(\epsilon) \approx \sigma^{-1}(\mathbf{0}) + \nabla \sigma^{-1}(\mathbf{0})^T \epsilon$ where $\sigma^{-1}(\cdot)$ is a element-wise function. Plugging into (14), we have

$$\begin{aligned}
(x' - x) &\approx U \text{diag}(g_c^{-1}(\lambda)) U^\top (\sigma^{-1}(\mathbf{0}) + \nabla \sigma^{-1}(\mathbf{0})^T \epsilon) \\
x' &\approx U \text{diag}(g_c^{-1}(\lambda)) U^\top \nabla \sigma^{-1}(\mathbf{0})^T \epsilon + U \text{diag}(g_c^{-1}(\lambda)) U^\top \sigma^{-1}(\mathbf{0}) + x
\end{aligned} \quad (15)$$

Hence, we can observe that the variance of x' is almost identical to the variance of $U \text{diag}(g_c^{-1}(\lambda)) U^\top \nabla \sigma^{-1}(\mathbf{0})^T \epsilon$ in an asymptotic sense.

$$\begin{aligned}
\text{Var}(x') &\approx (\partial \sigma^{-1})^2(0) \text{Var}(U \text{diag}(g_c^{-1}(\lambda)) U^\top \epsilon) \\
&\geq \text{Var}(U \text{diag}(g_c^{-1}(\lambda)) U^\top \epsilon).
\end{aligned} \quad (16)$$

The last inequality holds as our assumption on the inverse activation function. We will elaborate more details and explain why it is a reasonable condition.

Fact 2. If z is a Gaussian random variable, i.e., $z \sim \mathcal{N}(\mu, \Sigma)$, then $Az \sim \mathcal{N}(A\mu, A\Sigma A^T)$.

$$\begin{aligned}
\Delta &= U \text{diag}(g_c^{-1}(\lambda)) U^\top \epsilon \\
&= U \text{diag}(g_c^{-1}(\lambda)) \xi \quad (\text{denote } \xi = U^\top \epsilon).
\end{aligned}$$

Here, the distribution of ξ is same as ϵ 's due to the orthogonal matrix U and the rotation invariance of the Gaussian distribution. We refer the reader to Fact 2 for details. Hence, note that $y = \text{diag}(g_c^{-1}(\lambda)) \xi$, we have

$$y \sim \mathcal{N}(0, \sigma^2 \text{diag}([(1 - \lambda_1)^{-2}, \dots, (1 - \lambda_N)^{-2}])).$$

$$\text{Var}(x') = \text{Var}(\Delta) = \sigma^2 \sum_{i=1}^N \frac{1}{(1 - \lambda_i)^2}.$$

Since the eigenvalue of the normalized Laplacian matrix is bounded, that is, $\lambda_i \in [0, 2], \forall i \in [N]$, we have $1 - \lambda_i \in [-1, 1]$ and $\frac{1}{(1 - \lambda_i)^2} \in [1, +\infty)$. It was worthwhile mentioning that the equality holds only when $\lambda_i = 0$ or $2, \forall i \in [N]$. Therefore,

$$\text{Var}(x') = \sigma^2 \sum_{i=1}^N \frac{1}{(1 - \lambda_i)^2} \geq N\sigma^2 = \text{Var}(\epsilon).$$

Regarding the condition $\partial\sigma^{-1}(0) \geq 1$, we can consider three representative examples to corroborate our assumption, i.e.,

- Sigmoid function; $\sigma(x) = \frac{1}{1+e^{-x}}$ and its inverse operator $\sigma^{-1}(x) = -\ln\left(\frac{1}{x} - 1\right)$. Thus, we have

$$\partial\sigma^{-1}(x) = \frac{1}{x - x^2},$$

and $(\partial\sigma^{-1}(x))^2 \rightarrow +\infty$ when x goes to zero.

- Hyperbolic tangent (Tanh) activation function; $\sigma(x) = \frac{e^x - e^{-x}}{e^x + e^{-x}}$. The inverse hyperbolic tangent is given as

$$\sigma^{-1}(x) = \frac{1}{2}[\ln(1+x) - \ln(1-x)].$$

Computing its gradient, we have

$$\partial\sigma^{-1}(x) = \frac{1}{1-x^2} \geq 1.$$

- Leaky ReLU;

$$\sigma(x) = \begin{cases} x & \text{if } x > 0 \\ \frac{x}{\alpha} & \text{if } x \leq 0, \end{cases} \Rightarrow \sigma^{-1}(x) = \begin{cases} x & \text{if } x > 0 \\ \alpha x & \text{if } x \leq 0, \end{cases}$$

where α is a constant belonging to $(1, +\infty)$. Therefore, the subgradient of σ^{-1} is larger or equal to 1.

□

Remark 3. *The last equality is extremely hard to hold in practice and indeed to corroborate our empirical finding that the inverse operator will amplify the noise.*

This concludes the proof of proposition 1. Next, we show proposition 1 still holds if GCN model is parameterized.

Parameterized Model We consider

$$\hat{h} = \sigma(WU \text{diag}(g_c(\lambda))U^\top x) + \epsilon, \quad (17)$$

where ϵ is the white Gaussian noise (i.e., $\epsilon \sim \mathcal{N}(0, \sigma^2 \mathbb{I}_N)$). Under the condition that W is orthogonal, the inverse operator admits

$$x' = U \text{diag}(g_c^{-1}(\lambda))U^\top W^\top \sigma^{-1}(\hat{h}). \quad (18)$$

Therefore,

$$\begin{aligned} x' &= U \text{diag}(g_c^{-1}(\lambda))U^\top W^\top \sigma^{-1}(\hat{h}) \\ &= U \text{diag}(g_c^{-1}(\lambda))U^\top W^\top \sigma^{-1}(\sigma(WU \text{diag}(g_c(\lambda))U^\top x) + \epsilon) \\ &= x + U \text{diag}(g_c^{-1}(\lambda))U^\top W^\top \sigma^{-1}(\epsilon). \end{aligned}$$

It was worth noting that the product of orthogonal matrices is orthogonal. By the similar argument in Proposition 1, we can also conclude that the proposed inverse operation may introduce undesirable noise into the output graph.

B Comparisons with Additional Baselines

We additionally provide the comparison results of our method with three discrete matrix completion models: sRGCNN [29], GC-MC [4], and GraphRec [12]. We adapt the same setting as in Section 4.1 and the results are shown in Table 5. Ours yields the smallest imputation error on all datasets compared with the three matrix completion models. Notice that the three matrix completion models are specially designed for discrete matrix completion, where ours is applicable to both continuous and discrete feature values.

C Graph Autoencoder Framework

C.1 Encoder

Our encoder consists of two layers of Graph Convolutional Networks (GCN) [20], to produce smoothed representations of the input graphs.

Convolution

$$H = \text{GCN}(A, X), \tag{19}$$

where $H \in \mathbb{R}^{N \times v}$ denotes smoothed node representations.

C.2 Decoder

Our decoder consists of one layer of GDN, to produce fine-grained graphs.

Deconvolution

$$X' = \text{GDN}(A, H), \tag{20}$$

where $X' \in \mathbb{R}^{N \times d}$ denotes the recovered graph features.

C.3 The loss function

The reconstruction loss is a feature reconstruction loss.

$$\mathcal{L} = f(X, X'), \tag{21}$$

where $f(\cdot, \cdot)$ denotes a differential distance metric, e.g., $f(\cdot, \cdot) = \text{MSE}(\cdot, \cdot)$, and $\text{MSE}(\cdot, \cdot)$ represents Mean Squared Error.

D Detailed Model Configuration

All the experiments are done on a single machine with 32 cores and 300G memories. We don't use GPU as it involves a lot of sparse matrix multiplication.

For graph feature imputation, We use the graph autoencoder framework specified in Appendix C. The recovered graph features X' is used to infer the potential missing features. We train our model using Adam optimizer with a learning rate of $\{0.005, 0.002\}$. The output dimension of the first layer is $\{256, 512\}$. The output dimension of the second layer is 128. The number of epochs is chosen from $\{100, 200\}$. We use full-batch size. We stack the output of the first GCN layer and the second GCN layer in our encoders, and use left normalization to preprocess adjacency matrix. We don't use feature Dropout as it does not improve the performance. We use DropEdge [31]. We use grid search to choose the hyper-parameters. The selected parameters are reported in Table 6.

For graph generation, We strictly follow the architectures of VGAE [19] and Graphite [14] and add one feature reconstruction loss. The overall reconstruction loss is a sum of structure reconstruction term and feature reconstruction term,

$$\log p(G|Z) = \log p(A|Z) + \log p(X|Z), \tag{22}$$

where $p(A|Z)$ is the default structure reconstruction term such as a simple inner product of latent variables in VGAE, i.e., $\prod_i \prod_j p(A_{ij}|z_i, z_j)$. $\log p(X|Z)$ is computed with GDN and defined as

Table 5: RMSE test comparison with matrix completion methods on graph feature imputation

Datasets	Ciao	Douban	Cora	Citeseer	Amaphoto	Amacomp
sRGCNN [27]	1.183	0.801	0.550	0.551	0.519	0.591
GC-MC [3]	1.061	0.734	0.434	0.420	0.402	0.405
GraphRec [11]	1.062	0.754	0.437	0.425	0.417	0.417
OURS	1.011	0.734	0.415	0.399	0.391	0.393

Table 6: Summary of chosen hyper-parameters on graph feature imputation

Datasets	Ciao	Douban	Cora	Citeseer	Amaphoto	Amacomp
Dim of the first layer	256	256	512	256	256	256
Dim of the second layer	128	128	64	128	128	128
Learning rate	0.005	0.005	0.002	0.005	0.005	0.005
Epochs	200	200	200	200	100	100
DropEdge rate	1	0.5	0.5	0.5	1	1

in Eq. 21. As both VGAE and Graphite can only deal with homogeneous edge attribute, we don't differentiate bond types in ZINC dataset, i.e., we only evaluate if there is a bond between two given atoms. The number of epochs, initial learning rate and hyperparameters are all set to be the same with VGAE [19] or Graphite [14], for a fair comparison. The effect of orders of Maclaurin Series in GDN are reported in Table 7.

E Derivative of Inverse Operator

$$g_c^{-1}(\lambda_i) = \frac{1}{1 - \lambda_i} = \sum_{n=0}^{\infty} \frac{\left(\frac{1}{1-\lambda_i}\right)_{\lambda_i=0}^{(n)}}{n!} \lambda_i^n = \sum_{n=0}^{\infty} \frac{(-1)^n n! (-1)^n}{n!} \lambda_i^n = \sum_{n=0}^{\infty} \lambda_i^n$$

where (n) denotes the n -th order derivative. Thus, Eq. 9 can be obtained as:

$$U \text{diag}\left(\sum_{n=0}^{\infty} \lambda_1^n, \dots, \sum_{n=0}^{\infty} \lambda_N^n\right) U^\top = U \sum_{n=0}^{\infty} \Lambda^n U^\top \tag{23}$$

Table 7: Summary of the effect of orders of Maclaurin Series in GDN on the performance of graph structure generation

Datasets		MUTAG			PTC-MR			ZINC		
-	$\log p(A Z)$	AUC	AP	$\log p(A Z)$	AUC	AP	$\log p(A Z)$	AUC	AP	
VGAE + GDN	First-order	-1.002	0.738	0.464	-1.351	0.493	0.386	-0.999	0.474	0.239
	Second-order	-1.008	0.766	0.502	-1.356	0.559	0.443	-1.001	0.611	0.345
	Third-order	-1.026	0.823	0.611	-1.351	0.760	0.602	-1.006	0.858	0.611
Graphite + GDN	First-order	-1.003	0.741	0.470	-1.355	0.529	0.398	-1.001	0.478	0.241
	Second-order	-1.014	0.774	0.501	-1.358	0.574	0.450	-1.003	0.632	0.379
	Third-order	-1.024	0.818	0.608	-1.347	0.773	0.613	-0.998	0.838	0.567